Aerosol Impacts on the Diurnal Cycle of Marine Stratocumulus

IRINA SANDU, JEAN-LOUIS BRENGUIER, OLIVIER GEOFFROY, ODILE THOURON, AND VALERY MASSON

CNRM-GAME, Météo-France, CNRS, Toulouse, France

(Manuscript received 9 March 2007, in final form 27 November 2007)

ABSTRACT

Recent large-eddy simulation (LES) studies of the impact of aerosol on the dynamics of nocturnal marine stratocumulus revealed that, depending on the large-scale forcings, an aerosol-induced increase of the droplet concentration can lead to either an increase or a decrease of the liquid water path, hence contrasting with the cloud thickening that is expected from a reduction of the precipitation efficiency. In this study, the aerosol impacts on cloud microphysics are examined in the context of the boundary-layer diurnal cycle using 36-h LES simulations of pristine and polluted clouds. These simulations corroborate previous findings that during nighttime aerosol-induced liquid water path changes are sensitive to the large-scale forcings via enhancement of cloud-top entrainment such that, ultimately, the liquid water path may be reduced when the free-tropospheric-entrained air is drier. During the day, however, enhanced entrainment, inhibition of drizzle evaporation below cloud base, and reduced sensible heat flux from the surface lead to a more pronounced decoupling of the boundary layer, which significantly amplifies the liquid water path reduction of the polluted clouds. At night the sign of the liquid water path difference between pristine and polluted clouds depends upon large-scale forcings, while during the day the liquid water path of polluted clouds is always smaller than the one of the pristine clouds. Suggestions are made on how observational studies could be designed for validation of these simulations.

1. Introduction

The ability of aerosol particles to act as cloud condensation nuclei (CCN) has been extensively documented since the late 1950s and the 1960s. Gunn and Phillips (1957), Squires (1958), Squires and Twomey (1961), Warner (1968), and Warner and Twomey (1967) pointed out that high CCN concentrations from anthropogenic sources, such as from industrial pollution and the burning of sugarcane, can increase cloud droplet number concentration (CDNC), hence increasing cloud microphysical stability and potentially reducing precipitation efficiency. Twomey (1977) also anticipated that a CDNC increase at constant liquid water path (LWP) should result in an increase of the cloud albedo. This is currently referred to as the first aerosol indirect effect (AIE). It took, however, more than 20 years to corroborate this hypothesis through satellite observations of ship tracks (Coakley et al. 1987; Radke et al. 1989; King et al. 1993; Ferek et al. 1998; Durkee et al. 2000, 2001). The Twomey hypothesis was further corroborated in extended cloud systems affected by anthropogenic pollution, using two instrumented aircrafts for independent measurements of cloud microphysics in situ and remote sensing of cloud radiative properties from above the cloud layer (Brenguier et al. 2000) or using ground remote sensing (Feingold 2003). Recently, Boers et al. (2006) and Bennartz (2007) were able to retrieve, from satellite-measured radiances, seasonal and latitudinal variations of cloud albedo directly connected to CCN and CDNC changes.

The main obstacle in the experimental assessment of the first AIE is that the LWP is a highly variable parameter in clouds that impacts cloud albedo more efficiently than CDNC changes (Boers and Mitchell 1994; Brenguier et al. 2000). It is therefore difficult to distinguish cloud albedo variations caused by aerosol changes from those caused by the LWP natural variability. Moreover, it is difficult to observe the first AIE only because droplet concentration changes are also likely to affect cloud dynamics via modifications of radiative transfer and precipitation efficiency (Gunn and Phillips 1957; Albrecht 1989). In the framework of climate change, the bulk of the attention, therefore,

Corresponding author address: Irina Sandu, CNRM-GAME, Météo-France, 42 avenue G. Coriolis, 31057 Toulouse, France.
E-mail: irina.sandu@cnrm.meteo.fr

DOI: 10.1175/2008JAS2451.1

© 2008 American Meteorological Society

moved to the second aerosol indirect effect, that is, on aerosol-induced changes of cloud dynamics and cloud cover and the corresponding impacts on the earth radiation budget and hydrological cycle.

Marine boundary layer clouds, such as stratocumulus, are well suited for studies of the second AIE for numerous reasons: (i) They cover a large fraction of the planetary ocean [~30% according to Warren et al. (1988)]. Despite their small liquid water content (LWC), their albedo is about 10 times greater than the one of the underlying dark ocean surface. Their negative radiative contribution is, therefore, a crucial component of the earth radiation budget (Hartmann et al. 1992). (ii) Anthropogenic aerosol sources affect primarily the boundary layer, hence CDNC in boundary layer clouds. (iii) Boundary layer clouds have a lower optical thickness than deep convective clouds, hence a greater sensitivity of cloud albedo to aerosol-induced optical thickness changes. (iv) Because they are thinner than deep convective clouds, the maximum mean volume droplet diameter in the layer is less likely to reach the value of 32 μm, considered by Gerber (1996) as a threshold for the onset of precipitation. So a slight CDNC increase, hence droplet size decrease at constant LWC, is more likely to inhibit precipitation.

A fundamental component of the stratocumulus-topped boundary layer (STBL) is its diurnal cycle. Numerous studies based on 1D models (Nicholls 1984; Bougeault 1985; Turton and Nicholls 1987), 3D large-eddy simulations (LES) (Duynkerke et al. 2004), and field experiments, such as the First International Satellite Cloud Climatology Project (ISCCP) Regional Experiment (FIRE, 1987) (Betts 1990; Hignett 1991), the Atlantic Stratocumulus Transition Experiment (ASTEX, 1992) (Ciesielski et al. 2001), and the East Pacific Investigation of Climate (EPIC, 2001) (Bretherton et al. 2004), established that the STBL shows noticeable variations over a 24-h cycle: during nighttime the cloud layer gets thicker and the STBL is well mixed, while during daytime the cloud layer is partly decoupled from the surface layer, causing the cloud layer to become thinner (Nicholls 1984). The key process controlling this diurnal cycle is the cloud–radiation interaction (Nicholls 1984; Ciesielski et al. 2001). However, several additional processes modulate such interactions. These include precipitation (Paluch and Lenschow 1991; Stevens et al. 1998; Lu and Seinfeld 2005) and variations in the larger-scale conditions (Bretherton and Wyant 1997; Jiang et al. 2002; Ackerman et al. 2004; Lu and Seinfeld 2005).

Observational studies of the second AIE are challenging because boundary-layer air masses that exhibit different aerosol properties usually have different histories, which lead to systematic differences in the meteorology, making it difficult, if not impossible, to isolate the effect of the aerosol. Measurements of the large-scale forcings are not accurate enough, and our understanding of the dynamics of stratocumulus is not complete enough, to precisely predict what the LWP of a cloud layer should be. To illustrate this drawback, consider a STBL with a cloud base temperature of about 20°C and a cloud thickness of 100 m. The total (vapor plus liquid) water content is of the order of 20 g m^{-3} whereas the maximum (adiabatic) LWC at cloud top reaches only 0.2 g m^{-3}, that is, 1/100 of the total. To predict LWC variations with a relative accuracy of 1/10 would therefore require capabilities to measure the total water content with a relative accuracy of 1/1000 and temperature, which determines the saturation mixing ratio, with an absolute accuracy of 0.065°C, which is far beyond the actual performance of airborne or radiosounding instruments. Another illustration is the second Aerosol Characterization Experiment (ACE-2), which provided eight case studies of stratocumulus cloud layers with CDNC values ranging from 50 to 250 cm^{-3}. The cloud albedo of the most polluted cases, despite their higher CDNC, was lower than the one of the pristine cases. Indeed, the most polluted cases were characterized by thinner clouds (Brenguier and Pawlowska 2003). This feature might be interpreted as the signature of a negative second AIE. The most reasonable explanation, however, was that polluted air masses had crossed the Iberian Peninsula and experienced reduced latent and increased sensible heat fluxes compared to the pristine air masses that were flowing over the ocean for about a week before reaching the area of the field experiment, north of the Canary Islands.

Given the complex interactions governing the STBL and the difficulties in precisely measuring its governing physical parameters, the study of the second AIE calls for the use of high-resolution (LES) numerical models with state-of-the-art parameterizations of cloud dynamics, turbulence, radiation, and microphysics. Even though larger-scale forcings cannot be determined with sufficient accuracy, they can be tuned for the model to reproduce the expected cloud structure. It is then postulated that, if the external forcings are kept unchanged while modifying aerosol properties, the model is able to capture the essence of the interactions between the aerosol and the physical processes that influence the cloud life cycle. The numerical simulations can then be analyzed to identify measurable signatures of the second AIE.

The LES technique was applied in recent studies to examine the second AIE (Stevens et al. 1998; Acker-

man et al. 2003, 2004; Lu and Seinfeld 2005). Based on their analysis, Stevens et al. (1998) suggested that the response of stratocumulus to an increased aerosol loading may be more complex than predicted by Pincus and Baker (1994), a suggestion born out in subsequent studies (e.g., Ackerman et al. 2004; Lu and Seinfeld 2005). Depending on the dynamical feedbacks induced by the interactions between radiation and processes, such as drizzle precipitation, cloud droplet sedimentation, and entrainment at cloud top, and their sensitivity to the large-scale state of the atmosphere (e.g., as manifest in the thermal structure of the free troposphere, subsidence rates, or sea surface temperatures), the LWP may either increase or decrease following a CDNC increase. These results indicate that the question of how the aerosol impacts on the stratocumulus life cycle remains an open one, notwithstanding attempts to incorporate preconceived effects into general circulation models [for instance, for the purposes of the Fourth Assessment Report of the Intergovernmental Panel on Climate Change (IPCC) (Solomon et al. 2007)].

Most of the recent studies examined the short time STBL response to variations of the aerosol loading (a few hours, covering nighttime or daytime periods). The simulations suggested that the cloud sensitivity to CDNC variations is reduced during daytime because of the absorption of solar radiation in the cloud layer (Ackerman et al. 2003, 2004; Lu and Seinfeld 2005). Following Lu and Seinfeld (2005), who recommended examination of the coupling between aerosol indirect effects and the diurnal cycle, LES is used here to simulate a diurnal cycle of marine stratocumulus. The large-scale forcings are tuned for the cycle to be periodic in pristine conditions; that is, $\mathrm{LWP}(t) \approx \mathrm{LWP}(t + 24)$. The simulation is then repeated but, after the spinup period, the CCN concentration is increased to simulate polluted conditions.

The model is described in the next section and the simulations are presented in section 3. The aerosol impacts on the physical processes and the coupling with the diurnal cycle are discussed in section 4. The sensitivity of the results to the large-scale forcings is examined in section 5. In section 6, the results are summarized and suggestions are offered for using observations to test the insights we develop.

2. Description of the LES model

The nonhydrostatic model Meso-NH (Lafore et al. 1998) has been designed to simulate air motions over a broad range of scales ranging from the synoptic scale to turbulent eddies. The Meso-NH configuration chosen here for LES modeling of marine stratocumulus uses an anelastic system of equations (Lipps and Hemler 1982) and a 3D turbulence scheme with a 1½-order closure, that is, prognostic turbulent kinetic energy (TKE) and a diagnostic mixing length (Deardorff 1980). The conservative variables, liquid water potential temperature θ_l, and total water mixing ratio q_t are advected with a positive definite second-order centered scheme.

The surface sensible (H) and latent (LE) heat fluxes are proportional to the difference in temperature and specific humidity between the ocean and the air just above the surface:

$$H = \rho_a C_p C_H V_a (T_s - T_a),$$
$$LE = L_v \rho_a C_H V_a (q_{\mathrm{sat}}(T_s) - q_a), \quad (1)$$

where ρ_a, T_a, and q_a represent, respectively, the density, the temperature, and the specific humidity of the air situated above the surface; V_a is the wind speed at the surface, T_s is the ocean temperature, and $q_{\mathrm{sat}}(T_s)$ is the specific humidity at saturation. The constants L_v and C_p represent the enthalpy of vaporization and the isobaric specific heat capacity, respectively. The coefficient of proportionality C_H is derived by taking into account the thermodynamic stability above the surface F_H and the roughness length z_0 [given by Charnock (1955), i.e., $C_H = F_H(k_0/l_n(z/z_0))$], with k_0 representing the von Kármán constant.

The model includes a two-moment bulk microphysical scheme based on the parameterization of Khairoutdinov and Kogan (2000, hereafter KK2000), which was specifically designed for LES studies of warm stratocumulus clouds. The radiative transfer is computed using the European Centre for Medium-Range Weather Forecasts operational model radiation code (Morcrette 1991).

a. Microphysical scheme

Four prognostic variables are used for the condensed water: the cloud droplet and drizzle drop concentrations (N_c and N_r) and the cloud water and drizzle mixing ratios (q_c and q_r). Autoconversion, accretion, drizzle sedimentation, and evaporation are parameterized following KK2000 (their Eqs. 29, 33, 37 and 22, respectively). The limit between droplets and drizzle drops is set to 50 μm in diameter.

A fifth prognostic variable is used to account for already activated CCNs, following the activation scheme of Cohard et al. (1998). This scheme may be seen as an extension of the Twomey (1959) parameterization for more realistic activation spectra. The number of CCN, activated at any time step, is equal to the difference between the number of CCN, which would activate at the diagnosed pseudoequilibrium peak supersaturation in the grid, and the concentration of already activated

CCN (N_a). The aerosols are assumed to be lognormally distributed. The CCN activation spectrum is prescribed as

$$N_a = Cs_{v,w}^k F\left(\mu, \frac{k}{2}, \frac{k}{2}+1, \beta s_{v,w}^2\right), \quad (2)$$

where C is the concentration of activated CCN at a very high (infinite) supersaturation, $s_{v,\omega}$ is the pseudoequilibrium peak supersaturation (%), and $F(a, b, c, x)$ is the hypergeometric function (Press et al. 1992); k, μ, and β are parameters that can be tuned to represent various aerosol types (Cohard et al. 2000). The model offers thus the possibility to vary both the CCN type and their number concentration. Anthropogenic sulfates were chosen here for the entire set of simulations ($k = 1.4$, $\beta = 25.5$, $\mu = 0.834$).

The condensation/evaporation rate is derived using the Langlois (1973) saturation adjustment scheme. The cloud droplet sedimentation is computed by considering a Stokes law for the cloud droplet sedimentation velocity and assuming that the cloud droplet size distributions follow a generalized gamma law whose parameters were adjusted using droplet spectra measurements from the ACE-2 database ($\nu = 2$, $\alpha = 3$) (Pawlowska and Brenguier 2003; Geoffroy 2007); that is,

$$n_c(D) = N_c \frac{\alpha}{\Gamma(\nu)} \lambda^{\alpha\nu} D^{\alpha\cdot(\nu-1)} \exp[-(\lambda D)^\alpha], \quad (3)$$

where $\Gamma(x)$ is the gamma function, D is the cloud droplet diameter, and N_c is the CDNC. The parameter λ is given by

$$\lambda = \left[(\pi/6)\rho_w \frac{\Gamma(\nu + 3/\alpha)}{\Gamma(\nu)} \frac{N_c}{\rho_a q_c}\right]^{1/3},$$

where ρ_w and ρ_a are the densities of liquid water and of air, respectively, and q_c is the cloud water mixing ratio.

b. Radiative scheme

The radiative package is based on a two-stream formulation that solves separately the longwave (LW) and shortwave (SW) radiative transfers for independent model columns. The radiative fluxes are computed taking into account the absorption–emission of the LW radiation and the reflection, scattering, and absorption of solar radiation by the atmosphere and the earth's surface (Morcrette 1991). The radiative transfer is parameterized with a broadband flux emissivity method in the LW (Morcrette et al. 1986); the delta-Eddington approximation is used for the SW (Joseph et al. 1976).

The cloud LW optical properties are computed using the Savijärvi and Räisänen (1998) parameterization. In the SW, the cloud optical thickness is computed following Fouquart (1988) as a function of the LWP and of the cloud droplet effective diameter d_{eff}, $\tau = 3\text{LWP}/4\rho_w d_{\text{eff}}$, where ρ_w is the water density. The asymmetry factors in the visible and near-infrared ranges of the spectrum are set to 0.85 and 0.92, respectively. The single scattering albedo corresponds to cloud droplets formed on sulfates. The absorption coefficient of sulfate is low (10^{-7} at a wavelength of 500 nm), similar to that of pure water. An aerosol with a low absorption coefficient is selected here to avoid concomitant impacts owing to aerosol-absorbing properties (the semidirect effect), which are beyond the purpose of this study.

3. The impact of the droplet concentration on the cloud diurnal cycle

a. Setup of the simulations

The simulations carried out in this study correspond to a typical summer situation over the northeast Pacific. A study by Wood et al. (2002), based on satellite radiances gathered over a 3-yr period, shows that over this region marine stratocumulus have a diurnal mean LWP of approximately 60–70 g m^{-2}. To simulate a persistent cloud layer with such characteristics, meteorological conditions similar to that observed during the FIRE-I are selected.

The model initialization follows the setup of the intercomparison study performed during the European Project on Cloud Systems (EUROCS) (Duynkerke et al. 2004), with the same values of sea surface temperature, horizontal wind speed, inversion layer altitude (~600 m MSL), total water mixing ratio (q_t) vertical profile, and θ_l and q_t jumps at cloud top (12 K and -3 g kg^{-1}). To simulate a deeper cloud however, with significant precipitation at low CDNC, the initial liquid water potential temperature (θ_l) profile was set 1 K cooler than prescribed in EUROCS.

The subsidence rate is computed as $\overline{w_{\text{subs}}} = -Dz$ (s^{-1}) with a constant divergence rate D of 6×10^{-6} s^{-1}. This divergence rate is close to the average value indicated by Neiburger (1960) for the San Nicholas Island cases. No large-scale advection by the horizontal winds was considered in the reference case (hereafter W6).

To simulate the aerosol impact on CDNC, the Cohard et al. (2000) scheme is initialized with increasing values of the C coefficient, producing (at infinite supersaturation) concentrations of activated nuclei of 50, 200, and 600 cm^{-3}, respectively. The corresponding simulations are referred to as N_{CCN}^{50}, N_{CCN}^{200}, and N_{CCN}^{600} hereafter. The droplet concentration, however, does not increase proportionally to the CCN concentration.

Indeed, as the vertical velocity in stratocumulus clouds is moderate (less than 1 m s^{-1}), the enhanced competition for water vapor induced by an increased CCN concentration limits the in-cloud peak supersaturation. So, the peak supersaturation reaches values of the order of only 0.1% in the polluted cases, compared to 0.4% in the pristine case, thus limiting the number of CCN which form cloud droplets. The mean CDNC value, averaged over all model grids with CDNC >20 cm^{-3}, thus ranges from 38–40 cm^{-3} for N_{CCN}^{50}, to 100–135 cm^{-3} for N_{CCN}^{200}, and to 190–230 cm^{-3} for N_{CCN}^{600}.

The simulation for the pristine case starts at 2100 local time (LT) and lasts for 39 hours. During the first 3 h of simulation (spinup period), the LWP decreases rapidly from 230 to approximately 100 g m^{-2} at 0000 LT owing to relatively high drizzle rates (2 mm day^{-1}). After the spinup period, the pristine cloud LWP varies only slowly, showing that the simulation has reached a quasi-stationary state. The simulations for the polluted cases (N_{CCN}^{200} and N_{CCN}^{600}) start at 0000 LT, with the same field as the marine case at that time, and are run for 36 hours.

The domain size is 2.5 km × 2.5 km × 2 km for all simulations, with 50-m horizontal resolution and a constant vertical grid spacing of 10 m from the sea surface to the 850-m level that is above the inversion for all simulations. The vertical resolution is slightly decreased above this height, so 105 levels are used between the sea level and the top of the domain. The time step is of 1 s, and the lateral boundary conditions are periodic. The radiation code is called every 150 s for reducing the computational cost. The sensitivity to the size of the simulation domain was tested by simulating a pristine and a polluted diurnal cycle on a domain four times larger, that is, 5 km × 5 km × 2 km. The results showed that the evolution of the horizontal mean quantities (cloud depth, LWP, CDNC, rain rate, etc.) is not significantly influenced by the domain size. It appears that the reduced domain is able to capture the diurnal evolution of the mean structure of the STBL for both pristine and polluted cases. If simulations longer than 36 h were desirable, however, the domain would have to be extended because the turbulent structures in the boundary layer progressively grow with time.

b. Results

The time evolution of the domain-averaged LWP (g m^{-2}), plotted in Fig. 1a shows how strongly the CDNC changes affect the diurnal evolution of the cloud. The system response is nontrivial: During the first night of simulation, the LWP increases with increased CCN loading as expected, but this tendency is reversed after 1000 LT. Indeed, the two polluted clouds progressively thin relative to their pristine counter part during the last 26 h of the simulation. The cloud fraction, however, is close to 1 for all cases over the 36 h of simulation. To interpret the specific features of the pristine and polluted simulations, the various physical processes that govern the evolution of the STBL are examined in light of previous work in the next section.

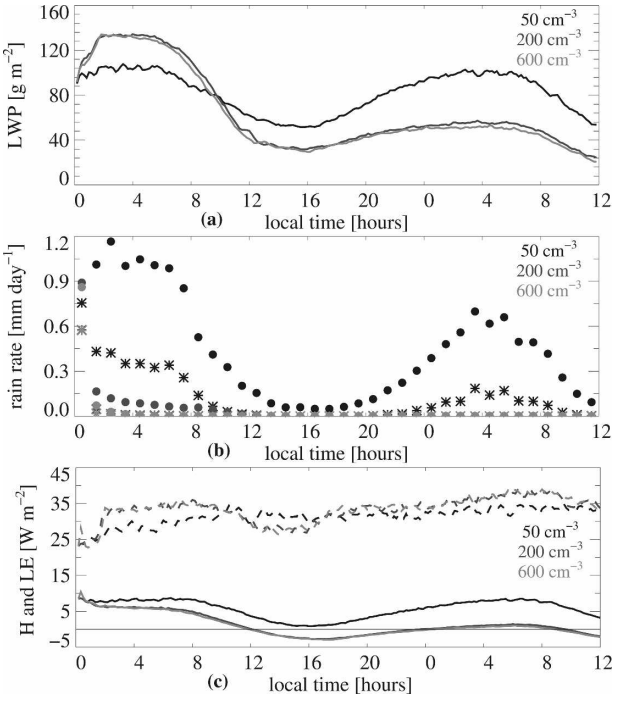

FIG. 1. Time evolution of the horizontal mean (a) LWP (g m^{-2}), (b) precipitation rates (hourly averages, mm day^{-1}) at sea level (stars) and at cloud base (dots), and (c) surface sensible (solid lines) and latent (dashed lines) heat fluxes. The black, dark gray, and light gray lines and symbols correspond to the N_{CCN}^{50}, N_{CCN}^{200}, and N_{CCN}^{600} simulations of the W6 case.

4. Discussion

a. Precipitation, cloud droplet sedimentation, and entrainment

The sudden change of the CCN concentration from 50 to 200 or to 600 cm^{-3}, imposed at 0000 LT, produces a rapid increase of the CDNC and a decrease of the domain-averaged droplet effective diameter at cloud top from 30 μm for the N_{CCN}^{50} case, to 22 μm for N_{CCN}^{200}, and to 17 μm for N_{CCN}^{600}. The autoconversion process is consequently inhibited [via the inverse dependence upon N_c in Eq. (29) of KK2000]. The precipitation rates, both at sea level and at cloud base, averaged over the domain (Fig. 1b) indicate that drizzle is almost completely suppressed about 1 h after the CCN concentra-

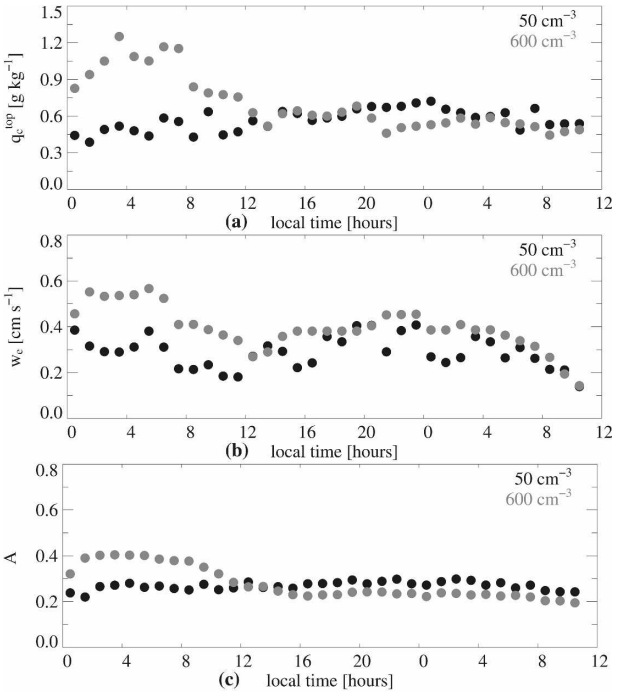

FIG. 2. Time evolution of the hourly averaged (a) horizontal mean cloud water mixing ratio (g kg^{-1}) integrated over the upper 30 m of the cloud layer, (b) entrainment velocity (m s^{-1}), and (c) entrainment efficiency [computed following Eq. (5) of Bretherton et al. (2007)]. The black and light gray symbols correspond to the N_{CCN}^{50} and N_{CCN}^{600} simulations of the W6 case.

tion increases. The polluted cases can, therefore, be considered as nonprecipitating cases, whereas the pristine one is continuously drizzling, albeit only marginally during the day. Because the two polluted cases respond similarly to the CDNC increase (Fig. 1a), the analysis, hereafter, will be mainly focused on the comparison of the pristine case N_{CCN}^{50} with the most polluted one N_{CCN}^{600}.

Because the cloud droplet diameter decreases with CDNC, the droplet sedimentation velocity is reduced. The inhibition of drizzle and the weaker cloud droplet sedimentation in the polluted clouds further results in higher water contents at cloud top. Figure 2a shows indeed that the polluted cloud N_{CCN}^{600} contains more water in its upper 30 m than the pristine one, especially during the first 11 h of simulation when its LWP is larger. Furthermore, the water content at its top remains equivalent to that of the pristine cloud, even when its LWP is almost halved relative to its pristine counter part (after 1200 LT). The domain-averaged vertical profiles of cloud water mixing ratio, plotted in Fig. 3a at 0900–1000 LT when the polluted and the pristine clouds have comparable LWPs, illustrate the effect of sedimentation on the vertical distribution of cloud water. Thus, the polluted cloud behaves like an adiabatically stratified cloud layer almost up to its top: the LWC increases linearly with height from the base to the top, and the LWP is proportional to the LWC at cloud top. In contrast, the divergent flux of liquid water substantially reduces the water content in the upper 60 m of the pristine cloud.

Over the years, a body of work has shown the entrainment rate to depend sensitively on the precipitation flux, both from drizzle or rain drops (Stevens et al. 1998; Stevens 2007) and from the sedimentation of cloud droplets (Ackerman et al. 2004; Bretherton et al. 2007). Although the different studies disagree on the character of the underlying mechanism, they agree on the effect, namely, that entrainment tends to be reduced in the presence of a divergent liquid water flux.

Our results are in accord with these earlier findings as the entrainment velocities are larger for the polluted (nonprecipitating) cloud, especially during the first 12 h of simulation (Fig. 2b). The entrainment velocities are computed here as the difference between the growth rate of the inversion level, that is, the first level above the cloud where the domain-averaged cloud water content becomes zero, and the large-scale subsidence. The significant intensification of entrainment noticed from 0000 to 1200 LT in the polluted case is consistent with the fact that the pristine case liquid water flux is maximum and, therefore, acts the most efficiently to reduce entrainment during the first night of simulation (Fig. 1b). Moreover, the behavior of the polluted cloud is correlated during this period with greater values of the entrainment efficiency, which is defined here following Eq. (5) of Bretherton et al. (2007; Fig. 2c). Although during these first 12 h the TKE values are not appreciably different in the polluted versus the pristine cases, this likely reflects enhanced fluctuations in the horizontal component of the TKE in the pristine case, consistent with more decoupling induced by drizzle evaporation under the cloud base. Comparisons of the vertical velocity variance show that the polluted case maintains more vigorous vertical overturning during the first night and the early morning (Fig. 3b), which is consistent with the development of a more well-mixed vertical structure (and hence better correspondence between LWC and LWP), more entrainment (Fig. 2b), and the development of a deeper PBL (Fig. 4). Moreover, despite its lower intensity during the last 24 h of simulation (Fig. 1b), the drizzle flux, as well as the flux of cloud water, act to stabilize and therefore weaken the vertical motions within the cloud layer, as suggested by Stevens et al. (1998). This tendency is illustrated by the slight reduction of the vertical velocity in the upper part of the pristine cloud both during daytime and during the following night (Fig. 3c). As a result, the cloud

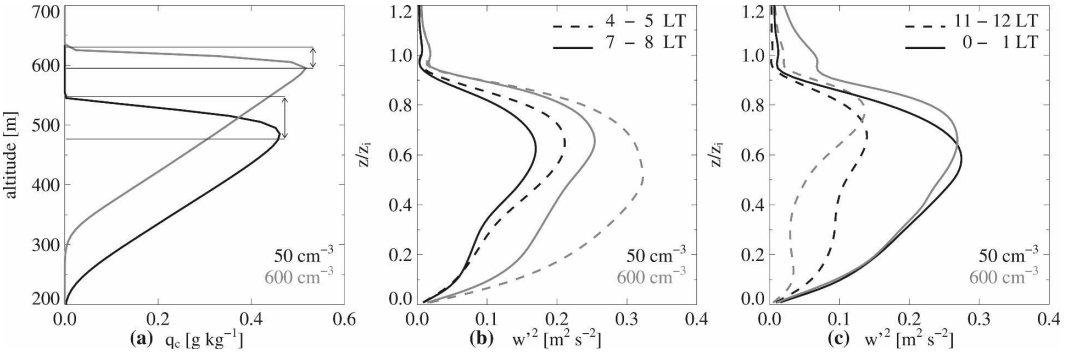

FIG. 3. (a) Vertical profiles of the horizontal mean cloud water mixing ratio, averaged between 0900 and 1000 LT when the polluted and the pristine clouds have comparable LWPs (g kg^{-1}). Hourly averaged variance of the vertical velocity (m^2 s^{-2}) as a function of altitude normalized by the height of the inversion level for (b) a nighttime (0400–0500 LT, dashed) and an early morning period (0700–0800 LT, full), and (c) a daytime (1100–1200 LT, dashed) and, respectively, a second nighttime period (0000–0100 LT, full). The black and the light gray lines correspond to the N_{CCN}^{50} and N_{CCN}^{600} simulations of the W6 case.

top entrainment is slightly damped compared to the polluted case during this period (Fig. 2b).

Our simulations corroborate Stevens et al. (1998) and Savic-Jovcic and Stevens (2008) findings about the different structures of precipitating and nonprecipitating stratocumulus. Thus, the precipitating cloud appears to be characterized by an "open cellular" structure associated with drizzle sedimentation, whereas the nonprecipitating one adopts a "closed cellular" morphology. Moreover, the up- and downdrafts are less frequent and weaker in the precipitating cloud through the entire simulation. This agreement with previous work suggests that despite its reduced size [100 times smaller than the one used by Savic-Jovcic and Stevens (2008) for their LES], our simulation domain is able to capture the different turbulent structures, hence the different time evolutions, of precipitating and nonprecipitating clouds.

These results present an increasingly familiar picture wherein precipitation leads to less entrainment and to a greater propensity toward decoupling or differentiation in the vertical structure of thermodynamic quantities. Furthermore, the polluted STBL is warmed and dried more efficiently than the pristine one through mixing with the overlying air. Beyond the intensification of cloud top entrainment, there are additional contrasting features of the pristine and polluted simulations, which also impact the LWP. They are discussed in the next section.

b. The coupling with the diurnal cycle

Both simulations start with the same vertical profiles at 0000 LT (dotted lines in Fig. 4). This profile is stable with slightly colder (Fig. 4a) and moister (Fig. 4b) air at the surface. This structure results from the spinup period (between 2100 and 0000 LT) during which CDNC

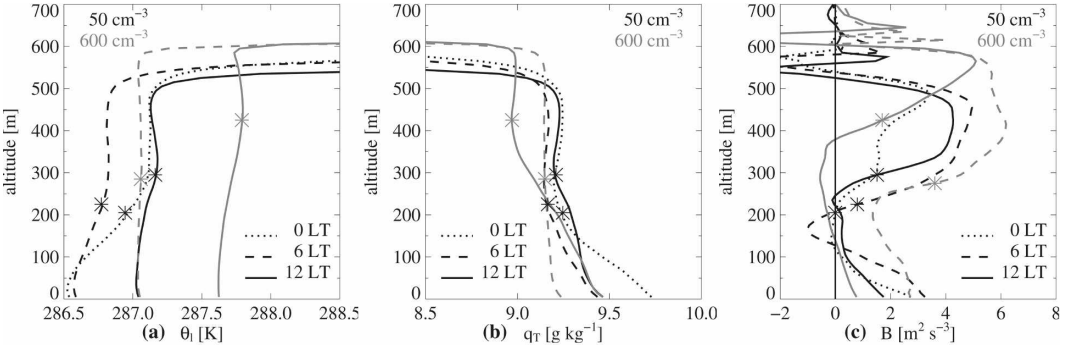

FIG. 4. Vertical profiles of the horizontal mean (a) liquid-water potential temperature (K), (b) total-water mixing ratio (g kg^{-1}), and (c) buoyancy flux ($B = \theta_v^{-1} g \overline{w'\theta_v'} \times 10^{-4}$ m^2 s^{-3}) at 0000 (dotted), 0600 (dashed) and 1200 LT (solid). The black and the light gray lines correspond to the N_{CCN}^{50} and N_{CCN}^{600} simulations of the W6 case; stars indicate the cloud-base altitude.

is low and a significant amount of liquid water is transported to the lower levels by precipitation.

During the first night (0000–0600 LT), the pristine cloud layer is progressively cooled by cloud-top LW radiative cooling, which drives turbulent circulations and mixes the layer. The turbulent eddies in turn cause cloud-top entrainment that, along with net condensation (measured by the precipitation reaching the surface) and surface heat fluxes, acts to warm the layer and counteract the cooling that drives the system in the first place. This compensation is not complete, so the liquid water potential temperature decreases through the course of this period (Fig. 4a). Most of the cooling is apparent in the cloud layer itself since during the same time period the layer is also mixing more effectively and tending toward a more well-mixed state. Below cloud base, drizzle evaporation in contrast slightly inhibits the mixing with the subcloud layer. This is reflected by the negative values of the buoyancy flux under the cloud base at 0600 LT (Fig. 4c).

Due to enhanced warming through cloud-top entrainment, which compensates more efficiently the radiative cooling, the polluted STBL cools less than the pristine layer during this first night (Fig. 4a). The more vigorous turbulence, which arises in the absence of drizzle, also maintains a more well mixed layer (Figs. 4a,b). The tendency of turbulence to be effective in mixing the layer is also evident in the buoyancy flux (Fig. 4c), which is positive through the entire polluted STBL at 0600 LT. The vertical mixing being stronger, the water vapor from the surface is more efficiently transported to the upper levels where it counteracts the drying due to cloud top entrainment (Fig. 4b). Because the more well mixed state is associated with warmer and drier subcloud layer air (Figs. 4a,b), the polluted case is characterized both by a slightly smaller surface sensible heat flux and by a stronger latent heat flux (Fig. 1c).

At 0600 LT, both clouds have about the same thickness, with higher cloud base and top altitudes for the polluted case and a significantly greater LWP because the LWC is everywhere greater in the polluted cloud than in the pristine one. The pristine STBL is still not perfectly coupled, whereas the polluted one is well mixed (Fig. 4c). The inhibition of drizzle and the strengthening of the turbulent mixing, which favors a more efficient transport of water vapor toward the cloud, have thus induced a greater LWP in the polluted case despite its stronger entrainment rate. At this stage, the simulation is in accord with the outline of Pincus and Baker's (1994) hypothesis, but the mechanism through which a reduction in cloudiness is achieved is somewhat different; that is, vertical stratification, which is not evident in the Pincus and Baker (1994) model, is central to the response of our simulations to changes in the aerosol loading.

After sunrise, from 0600 to 1200 LT, the situation evolves quite differently in the two cases: the diurnal cycle is damped in the pristine case relative to the polluted case, leading to more decoupling and less cloud in the latter. This is counter to naive expectations. In the pristine case, the sources in the θ_l budget (solar radiation absorption, cloud top entrainment, and latent heat release) outweigh the sinks (LW emission and droplet sedimentation), and the cloud layer is heated (Fig. 4a). During daytime, drizzle is not intense enough to reach the surface (Fig. 1b), but it remains effective in limiting entrainment and cooling the subcloud layer, destabilizing it with respect to the surface. The latter acts to compensate the radiative heating of the transition layer where the cloud base rises ~80 m between 0600 and 1200 LT (Fig. 4a). The net effect is to resist the tendency toward decoupling that would otherwise be expected to result from the effects of the solar radiative heating in the cloud layer. By 1200 LT the STBL is actually more well mixed than it was in the early morning period. This is especially evident in the profiles of total water mixing ratio (Fig. 4b), but also in the profile of buoyancy flux, which at 1200 LT is positive through the entire STBL (Fig. 4c).

During the same period, the polluted case experiences a contrasting evolution. The entrainment rate is still higher than in the pristine case (Fig. 2b) and the absorption of solar radiation is intensified by the greater values of the LWC at sunrise. Moreover, in the lack of drizzle, there is no heat sink to counterbalance the warming of the cloud base region. Besides, as the temperature above the surface gradually increases, the sensible heat flux rapidly decreases to reach slightly negative values at 1200 LT (Fig. 1c). While the subcloud layer is less heated by advection of warm air from the surface, the cloud layer is increasingly warmed by entrainment and absorption of solar radiation and begins to decouple from the surface (note the stratification developing at cloud base in Fig. 4a). The mixing between the surface and the cloud layer is further reduced by the decay of TKE thermal production close to the surface, caused by the lack of a significant sensible heat flux. The cloud layer thus gradually decouples from the surface, the buoyancy flux becoming negative over a 200-m layer below cloud base (Fig. 4c). This decoupling is manifest in the humidity field, which also tends to become increasingly stratified, "starving" the cloud layer of water (Fig. 4b). Consequently, the LWP sharply decreases in the morning and, finally at 1200

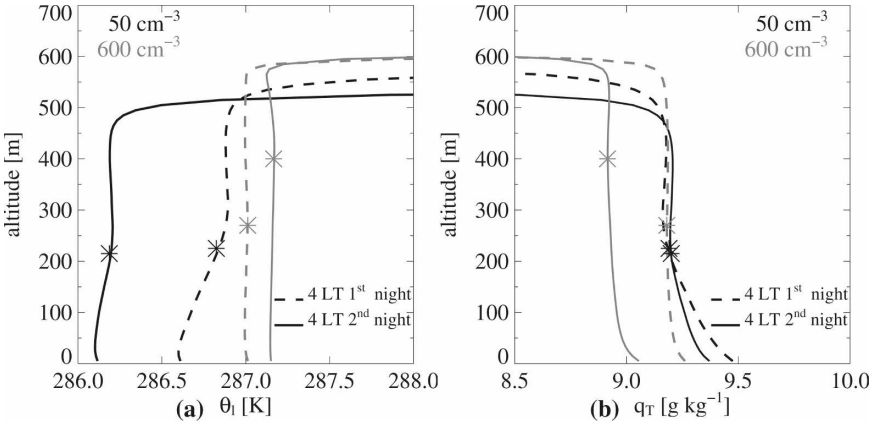

FIG. 5. Vertical profiles of the horizontal mean (a) liquid-water potential temperature (K) and (b) total-water mixing ratio (g kg^{-1}) at 0400 LT during the first (dashed) and the second (solif) nights of simulation. The black and light gray lines correspond to the N_{CCN}^{50} and N_{CCN}^{600} simulations of the W6 case; stars indicate the cloud-base altitude.

LT, it is much lower (30 g m^{-2}) than its pristine counterpart (Fig. 1a).

This evolution may be interpreted as the result of a coupling between increased entrainment rate at cloud top, stronger absorption of solar radiation into the cloud layer, the subsequent warming of the STBL, and attenuation of the surface sensible heat flux when the temperature at the lowest levels of the STBL approaches the surface temperature. The consequences are twofold: 1) the STBL gets warmer and drier, which reduces its LWP, and 2) the turbulence is no longer able to maintain a well-mixed state because of the significant negative buoyancy flux below cloud base. The absence of drizzle evaporative cooling in this region reinforces the decoupling. The moisture supply from the surface is cut off and the LWP is even more reduced than if the STBL was well mixed.

Once the LWP reaches its minimum at 1500–1600 LT, both the solar radiation and entrainment rate decrease, hence so does the warming and drying of the cloud layer. At this stage, one might expect that a neutral virtual temperature profile would be restored, that water vapor accumulated in the subcloud layer would progressively feed the cloud layer again, and that the cloud should be able to develop the same LWP as during the previous night. The examination of the 36-h simulations reveals, instead, that only the pristine case is able to restore the same LWP as during the first night.

After sunset (around 1800 LT), the shutdown of SW absorption and continuous LW cooling contribute to restore a well-mixed STBL in both simulations, and the cloud layers deepen (Fig. 1a). Figure 5 compares the θ_l and q_T vertical profiles at 0400 LT during the first and second nights. Over these 24 hours of simulation, the pristine STBL gets cooler. This indicates that LW cooling outweighed entrainment and surface sensible heat flux warming during this period. The STBL also becomes slightly shallower, which means that the 24-h averaged entrainment velocity is lower than the subsidence. Consequently, the resulting LWP values are similar on both nights. The polluted STBL, in contrast, gets warmer, significantly drier, and thicker, which implies that entrainment at cloud top is stronger than LW cooling and the entrainment velocity is greater than the subsidence. As a result, the LWP is much lower during the second night, reaching 50 versus 135 g m^{-2} at 0400 LT on the first night. Here we see that the long-term effect of less precipitation causes more entrainment; hence drying the layer leads, over long time periods, to fewer clouds, as hypothesized by Stevens et al. (1998).

These simulations suggest that, under large-scale conditions leading to a periodic diurnal cycle for pristine conditions, the addition of CCN particles and the resulting increase in CDNC drives the STBL into a nonreversible evolution so that the boundary layer does not restore the same liquid water path during the second night as during the first one.

5. Sensitivity to large-scale conditions

For the W6 case, no large-scale forcing was considered except a subsidence, which leads in the pristine case to a periodic diurnal cycle; that is, the cloud is able to produce the same LWP during the second night as during the first. To test the sensitivity of the pristine and polluted simulations to the large-scale forcings, the same exercise is now repeated with different condi-

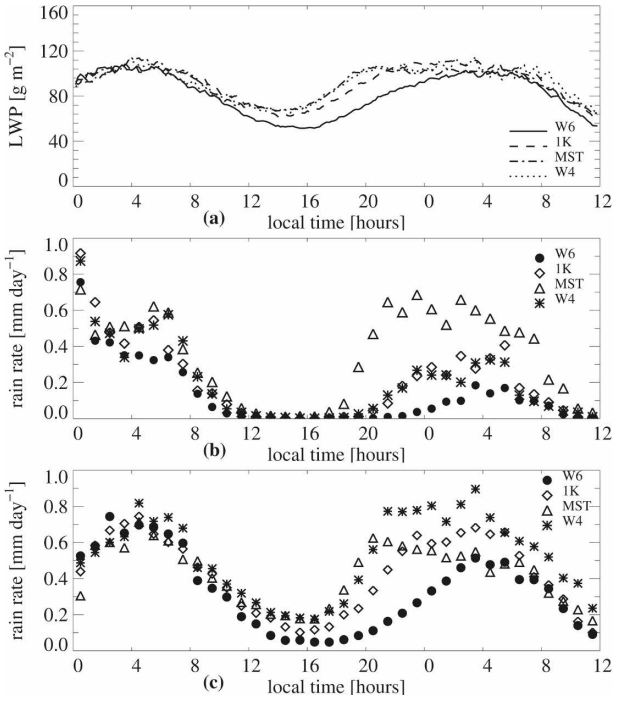

FIG. 6. Time evolution of the horizontal mean (a) LWP (g m^{-2}), (b) rain rate at the surface (hourly averages, mm day^{-1}), and (c) evaporated rain rate (hourly averages, mm day^{-1}) for the four pristine cloud simulations: W6 (solid/dots), 1K (dashed/diamonds), MST (dashed–dotted/triangles) and W4 (dotted/stars).

tions: The CCN concentration is still suddenly increased at 0000 LT from 50 to 600 cm^{-3} but the subsidence rate, large-scale advection, and inversion-layer moisture jump are modified in turn:

1) The first case (1K case) uses the same subsidence as for the W6 case except a continuous cooling of 1 K day^{-1}, accounting for horizontal advection of a colder air mass in the simulated domain, is applied;
2) The second case (MST case) is similar to W6 except for the humidity jump at the inversion level, which is reduced from -3 to -1 g kg^{-1};
3) For the third case (W4 case) the divergence used to compute the subsidence rate is reduced to 4×10^{-6} s^{-1}, the other conditions being similar to W6. This value is close to the divergence value retrieved for the FIRE-l case by Duynkerke and Hignett (1993).

First of all, we should note that all pristine simulations are continuously drizzling even if the drizzle flux weakens during daytime (Fig. 6b), whereas drizzle is always inhibited in the polluted simulations (not shown). Moreover, the moister inversion leads to less entrainment (MST case), the advection of a cooler air mass into the domain partially counters the gradual heating of the STBL (1K case), while the weaker subsidence favors a more pronounced raise of the cloud top (W4 case). So, one could expect that the new sets of large-scale forcings noticeably affect the LWP. This is not the case, however, for the pristine simulations. Figure 6a shows that, especially during nighttime, all pristine clouds show similar LWP. In fact, if the LWP increases owing to the imposed forcings, the rain rate is equally increasing and, hence, so does the amount of drizzle evaporating below cloud base (Figs. 6band 6c, from 1800 to 0400 LT). During the second night more water is thus lost by drizzle precipitation, and the enhanced drizzle rates inhibit in-cloud vertical motions (Stevens et al. 1998). Moreover, the intensified drizzle evaporation in the subcloud layer limits more efficiently turbulent mixing between the subcloud and the cloud layers. The transport of water vapor from the surface to the cloud layer is thus weakened, which further prevents the LWP from increasing.

During daytime (0900–1800 LT) though, when drizzle rates are weaker, the LWP is more sensitive to the large-scale conditions (Fig. 6a). It appears that, when drizzle evaporation below cloud base is intensified (Fig. 6c), the evaporative cooling balances more efficiently the SW absorption warming and limits the decoupling of the STBL. The diurnal reduction of the LWP is consequently smaller for the cases with enhanced drizzle evaporation (MST, W4, 1K). In summary, all pristine simulations show periodic diurnal cycles with amplitudes that are only slightly dependent on the large-scale forcings.

In the lack of drizzle, the polluted clouds are instead more sensitive to the large-scale forcings. Thus, the initial LWP increase is greater for the cases 1K, W4, and MST than for the reference W6 case. This feature is illustrated by the time evolution of the relative LWP difference between the polluted and the pristine cloud (in percents), shown in Fig. 7.

During daytime, however, the LWP of the polluted nonprecipitating clouds is rapidly reduced and tends to a minimum close to the one of the W6 polluted case. It appears that the bigger the LWP is at sunrise, the stronger the decoupling of the STBL is, and hence the LWP reduction and diurnal cycle amplitude. Indeed, the absorption of solar radiation into the cloud layer is proportional to the cloud water content, so, if the cloud is deeper at sunrise, it will be heated more strongly by the solar radiation. Moreover, even if the STBL is less heated by entrainment in the MST case and is kept cooler by the imposed 1 K day^{-1} cooling in the 1K case, the surface sensible flux decreases rapidly in all cases and reaches negative values around local noon. As ex-

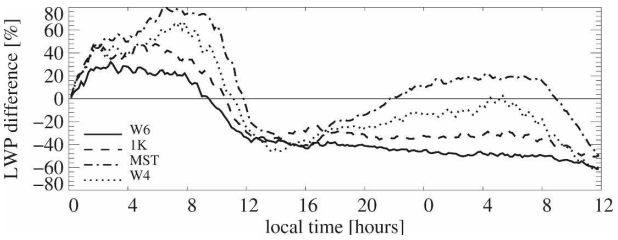

FIG. 7. Time evolution of the relative difference in horizontal mean LWP (%) between the polluted cloud N_{CCN}^{600} and the pristine cloud N_{CCN}^{50} for the four cases: W6 (solid), 1K (dashed), MST (dashed–dotted), and W4 (dotted). This difference was computed as the LWP difference between the two clouds, normalized by the LWP of the pristine cloud.

plained for the reference case, this results both in a reduction of turbulent mixing in the subcloud layer and in a slower warming of this layer compared to that of the cloud layer. This coupling between stronger solar absorption, cloud top entrainment, and reduced sensible heat flux amplifies the decoupling between the cloud and the subcloud layer. Thus, the polluted clouds always become thinner than the pristine ones during daytime, regardless of the imposed large-scale forcings.

During the second night, the LWP of the polluted clouds increases again, and the rate of increase is sensitive to the large-scale forcings. Thus, the polluted cloud LWP reaches the same peak value as the pristine one in the W4 experiment at 0500 LT, and it is greater in the MST experiment from 2200 to 0900 LT. Nevertheless, the heating and the drying of the polluted STBL leads in all cases to a nonreversible evolution; that is, the clouds never restore the same LWP during the second night as during the first.

The sensitivity of the simulation to the moment when the CCN concentration is increased has also been tested. If the concentration is increased during daytime (1200 LT) instead of 0000 LT, the initial LWP increase is no longer observed, but the polluted STBL exhibits the same evolution as in the W6 experiment. Thus, enhanced cloud top entrainment, solar radiation absorption, and the cutoff of the surface sensible flux get to a significant LWP reduction of the cloud until 1600 LT and, further, at nighttime values lower than the ones of the pristine cloud.

6. Summary and conclusions

Recent LES simulations of the aerosol impact on the LWP of marine boundary layer stratocumulus (Ackerman et al. 2004; Lu and Seinfeld 2005) demonstrated that, during nighttime, enhanced entrainment rate in the polluted cases may counteract, under specific large-scale conditions, the LWP increase expected from reduced drizzle precipitation rates. In fact, the LWP can be reduced instead of being increased as postulated by Pincus and Baker (1994). Meanwhile, Ackerman et al. (2004) and Lu and Seinfeld (2005) simulations suggested that during daytime the sensitivity of the STBL to CDNC changes is lower than during nighttime. In this study, similar LES simulations are used to examine the coupling between the impacts of CDNC changes and the diurnal cycle.

A 36-h simulation of a pristine stratocumulus diurnal cycle has first been performed with values of large-scale forcings such that the LWP during the second night is the same as during the first one. The simulation was then repeated, but after a spinup period of 3 h, the CCN concentration was suddenly increased so that the mean cloud droplet concentration also increased rapidly throughout the whole cloud layer.

The simulations reveal that, by inhibiting the sedimentation of liquid water, the CDNC increase leads to an intensified cloud top entrainment and also to a more efficient mixing of the STBL, hence a stronger transport of water vapor toward the cloud during the first night. So, the initial response of the STBL to a CDNC increase is an increase of the LWP. When the sun rises, however, the response is reversed and the LWP of the polluted clouds decreases more than its pristine counterpart. This evolution is mainly due to the enhanced entrainment rate at cloud top, but it is significantly reinforced by a decoupling of the STBL that results from absorption of solar radiation in the cloud layer (which is proportional to cloud water) and a reduction of the sensible heat flux from the surface. The pristine case is less affected because drizzle evaporative cooling in the upper part of the subcloud layer counteracts the heating by SW absorption and advection of warm air from the surface, hence damping the diurnal cycle. During the day, the pristine case is less decoupled and its LWP decreases less than the one of the polluted cases. During the following night, both the pristine and the polluted STBL become well mixed again and the LWP increases. The polluted case, which because of intensified entrainment warming and drying has a much higher cloud base, never reaches the same LWP values as during the first night. Its LWP remains much smaller than the one of the pristine cloud.

A sensitivity study to the large-scale forcings has also been performed with different values of the subsidence rate, the large-scale advective cooling, and the total water jump through the inversion. When the subsidence is reduced (W4 case), the LWP of the polluted cloud reaches the same value as the one of the pristine cloud during the second night and, when the tropospheric air

is moister (MST case), it even reaches a higher value. Overall, the sign and the amplitude of the LWP changes are only sensitive to the large-scale forcings during nighttime. During the day, our simulations suggest that the LWP response to a CDNC increase is always a reduction, irrespective of the large-scale forcings (within the range of values tested in this exercise). It seems that the processes responsible for the LWP reduction (enhanced cloud-top entrainment, SW absorption heating in the cloud layer, and reduced sensible flux from the surface) scale with the LWP maximum at 0600 LT. So, all polluted clouds tend toward the same LWP minimum at 1500 LT.

Our simulations suggest that, during daytime when the albedo of boundary layer stratocumulus significantly affects the earth radiative budget, polluted clouds should exhibit a lower LWP. Such a reduction of the LWP can be sufficient to counteract the increase of optical thickness owing to more numerous smaller droplets (Twomey effect), hence leading to an albedo comparable to that of pristine clouds growing in a similar (thermo)dynamical environment. This is the opposite of what was parameterized in climate models for the IPCC (Solomon et al. 2007). It is, therefore, crucial to corroborate such findings with observational studies of the second AIE.

The difficulties that we are facing, however, to show observational evidence of the second AIE are similar, in many ways, to the difficulties the weather modification community has been facing for more than 50 years. Indeed, we are still not able to characterize the thermodynamical environment of clouds with sufficient accuracy to predict what the LWP should be in pristine conditions, hence how it might be affected by aerosol changes. To bypass this obstacle, the weather modification community designed experiments with randomized cloud seeding though without success (International Aerosol Precipitation Scientific Assessment Group 2007). Such an approach is not applicable to anthropogenic inadvertent cloud modification since it might be quite difficult to randomize anthropogenic aerosol sources! LES simulations, however, provide some interesting insights and suggest new approaches for the validation of their results.

A first step might be to identify observable signatures of the aerosol impacts in the simulations. The most obvious one is the impact of CDNC on the vertical profile of LWC. All LES simulations of the second AIE mentioned herein show the same features, namely, that LWC profiles of polluted clouds are close to adiabatically stratified profiles up to cloud top, whereas in pristine clouds, the LWC profiles are noticeably subadiabatic in the upper 50 m below cloud top. Without such a feature, none of the LES models would predict enhanced entrainment at cloud top and reduced LWP in polluted clouds. We, therefore, suggest that previous experiment datasets [ACE-2 (Pawlowska and Brenguier 2000), EPIC (Bretherton et al. 2004; Comstock et al. 2007), and Second Dynamics and Chemistry of the Marine Stratocumulus field study (DYCOMS-II) (van Zanten and Stevens 2005; Stevens et al. 2003)] might be reanalyzed with a focus on the vertical profiles of LWC below cloud top. Other signatures of aerosol impacts are the enhanced variance of vertical velocity at cloud top in polluted clouds, the different morphologies of the upper cloud layer (closed versus open cells), and the amplitude of the diurnal cycle. In summary, even if we are not able to accurately predict from observations what a pristine or a polluted cloud LWP should be, there are observable features of LES simulations that are necessary for the models to simulate a reduction of the LWP in a polluted environment. Forthcoming field experiments should first focus on such features, like the LWC vertical profile at cloud top and some specific signatures in the turbulence field.

In a second step, one may also try to better constrain the simulations with more accurate datasets. If we can reduce the uncertainty on the large-scale forcings, statistical approaches might be successful for identifying aerosol impacts on the diurnal evolution of stratocumulus clouds. Our simulations suggest that such approaches should focus on the early morning part of the cycle during which cloud dynamics seems to be the most sensitive to the aerosol and droplet concentrations.

Acknowledgments. Irina Sandu acknowledges Météo-France's support of her Ph.D. in the GMEI group of CNRM. We are grateful to Bjorn Stevens for his thorough advice during the analysis of the simulations and his recommendations during the editorial process, which considerably improved the final manuscript. We also thank the three anonymous reviewers for their comments and suggestions.

REFERENCES

Ackerman, A. S., O. B. Toon, D. E. Stevens, and J. A. Coakley Jr., 2003: Enhancement of cloud cover and suppression of nocturnal drizzle in stratocumulus polluted by haze. *Geophys. Res. Lett.,* **30,** 1381, doi:10.1029/2002GL016634.

——, M. P. Kirkpatrick, D. E. Stevens, and O. B. Toon, 2004: The impact of humidity above stratiform clouds on indirect aerosol climate forcing. *Nature,* **432,** 1014–1017.

Albrecht, B., 1989: Aerosols, cloud microphysics, and fractional cloudiness. *Science,* **245,** 1227–1230.

Bennartz, R., 2007: Global assessment of marine boundary layer

cloud droplet number concentration from satellite. *J. Geophys. Res.,* **112,** D02201, doi:10.1029/2006JD007547.

Betts, A. K., 1990: Diurnal variation of California coastal stratocumulus from two days of boundary layer soundings. *Tellus,* **42A,** 302–304.

Boers, R., and R. M. Mitchell, 1994: Absorption feedback in stratocumulus clouds: Influence on cloud top albedo. *Tellus,* **46A,** 229–241.

——, J. R. Acarreta, and J. L. Gras, 2006: Satellite monitoring of the first indirect aerosol effect: Retrieval of the droplet concentration of water clouds. *J. Geophys. Res.,* **111,** D22208, doi:10.1029/2005JD006838.

Bougeault, P., 1985: The diurnal cycle of marine stratocumulus layer: A higher-order model study. *J. Atmos. Sci.,* **42,** 2826–2843.

Brenguier, J.-L, and H. Pawlowska, 2003: Cloud microphysical and radiative properties for parameterization and satellite monitoring of the indirect effect of aerosols on climate. *J. Geophys. Res.,* **108,** 8362, doi:10.1029/2002JD002682.

——, ——, L. Schuller, R. Preusker, J. Fischer, and Y. Fouquart, 2000: Radiative properties of boundary layer clouds: Droplet effective radius versus number concentration. *J. Atmos. Sci.,* **57,** 803–821.

Bretherton, C. S., and M. C. Wyant, 1997: Moisture transport, lower-tropospheric stability, and decoupling of cloud-topped boundary layers. *J. Atmos. Sci.,* **54,** 148–167.

——, T. Uttal, C. W. Fairall, S. E. Yuter, R. A. Weller, D. Baumgardner, K. Comstock, and R. Wood, 2004: The EPIC 2001 stratocumulus study. *Bull. Amer. Meteor. Soc.,* **85,** 967–977.

——, P. N. Blossey, and J. Uchida, 2007: Cloud droplet sedimentation, entrainment efficiency, and subtropical stratocumulus albedo. *Geophys. Res. Lett.,* **34,** L03813, doi:10.1029/2006GL027648.

Charnock, H., 1955: Wind stress over a water surface. *Quart. J. Roy. Meteor. Soc.,* **81,** 639–640.

Ciesielski, P., W. H. Schubert, and R. H. Johnson, 2001: Diurnal variability of the marine boundary layer during ASTEX. *J. Atmos. Sci.,* **58,** 2355–2376.

Coakley, J. J., R. Bernstein, and P. Durkee, 1987: Effects of ship-track effluents on cloud reflectivity. *Science,* **255,** 423–430.

Cohard, J.-M., J.-P. Pinty, and C. Bedos, 1998: Extending Twomey's analytical estimate of nucleated cloud droplet concentrations from CCN spectra. *J. Atmos. Sci.,* **55,** 3348–3357.

——, ——, and K. Shure, 2000: On the parameterization of activation spectra from cloud condensation nuclei microphysical properties. *J. Geophys. Res.,* **105,** 11 753–11 766.

Comstock, K., S. Yuter, R. Wood, and C. S. Bretherton, 2007: The three-dimensional structure and kinematics of drizzling stratocumulus. *Mon. Wea. Rev.,* **135,** 3767–3784.

Deardorff, J., 1980: Stratocumulus-capped mixed layers derived from a three dimensional model. *Bound.-Layer Meteor.,* **18,** 495–527.

Durkee, P. A., and Coauthors, 2000: Composite ship track characteristics. *J. Atmos. Sci.,* **57,** 2542–2553.

——, and Coauthors, 2001: The impact of ship-produced aerosols on the microstructure and albedo of warm marine stratocumulus clouds: A test of MAST hypotheses 1i and 1ii. *J. Atmos. Sci.,* **57,** 2554–2569.

Duynkerke, P. G., and P. Hignett, 1993: Simulation of diurnal variation in a stratocumulus-capped marine boundary layer. *Mon. Wea. Rev.,* **121,** 3291–3300.

——, and Coauthors, 2004: Observations and numerical simulations of the diurnal cycle of the EUROCS stratocumulus case. *Quart. J. Roy. Meteor. Soc.,* **130,** 3269–3296.

Feingold, G., 2003: Modeling of the first indirect effect: Analysis of measurement requirements. *Geophys. Res. Lett.,* **30,** 1997, doi:10.1029/2003GL017967.

Ferek, R., D. Hegg, and P. Hobbs, 1998: Measurements of ship-induced tracks in clouds off the Washington coast. *J. Geophys. Res.,* **103,** 199–206.

Fouquart, Y., 1988: Radiative transfer in climate modeling. *Physically-Based Modelling and Simulation of Climate and Climatic Changes,* M. E. Schlesinger, Ed., NATO Science Series C, Vol. 243, Springer, 1988 pp.

Geoffroy, O., 2007: LES modeling of precipitation in boundary layer clouds and parameterization for general circulation model (in French). Ph.D. thesis, Université Paul Sabatier, 220 pp.

Gerber, H., 1996: Microphysics of marine stratocumulus clouds with two drizzle modes. *J. Atmos. Sci.,* **53,** 1649–1662.

Gunn, R., and B. Phillips, 1957: An experimental investigation of the effect of air pollution on the initiation of rain. *J. Meteor.,* **14,** 272–280.

Hartmann, D., M. Ockert-Bell, and M. Michelsen, 1992: The effect of cloud type on earth's energy balance: Global analysis. *J. Climate,* **5,** 1281–1304.

Hignett, P., 1991: Observations of diurnal variation in a cloud-capped marine boundary layer. *J. Atmos. Sci.,* **48,** 1474–1482.

International Aerosol Precipitation Scientific Assessment Group, 2007: Aerosol pollution impact on precipitation: A scientific review. WMO/International Union of Geodesy and Geophysics, 482 pp.

Jiang, H., G. Feingold, and W. R. Cotton, 2002: Simulations of aerosol-cloud-dynamical feedbacks resulting from entrainment of aerosol into the marine boundary layer during the Atlantic Stratocumulus Transition Experiment. *J. Geophys. Res.,* **107,** 4813, doi:10.1029/2001JD001502.

Joseph, J. H., W. J. Wiscombe, and J. A. Weinman, 1976: The delta-Eddington approximation for radiative flux transfer. *J. Atmos. Sci.,* **33,** 2452–2459.

Khairoutdinov, M., and Y. Kogan, 2000: A new cloud physics parameterization in a large-eddy simulation model of marine stratocumulus. *Mon. Wea. Rev.,* **128,** 229–243.

King, M., L. Radke, and P. Hobbs, 1993: Optical properties of marine stratocumulus clouds modified by ships. *J. Geophys. Res.,* **98,** 2729–2739.

Lafore, J., and Coauthors, 1998: The Meso-NH Atmospheric Simulation System. Part I: Adiabatic formulation and control simulations. *Ann. Geophys.,* **16,** 90–109.

Langlois, W., 1973: A rapidly convergent procedure for computing large-scale condensation in a dynamical weather model. *Tellus,* **25,** 86.

Lipps, F., and R. S. Hemler, 1982: A scale analysis of deep moist convection and some related numerical calculations. *J. Atmos. Sci.,* **39,** 2192–2210.

Lu, M.-L., and J. H. Seinfeld, 2005: Study of the aerosol indirect effect by large-eddy simulation of marine stratocumulus. *J. Atmos. Sci.,* **62,** 3909–3932.

Morcrette, J.-J., 1991: Radiation and cloud radiative properties in the European Centre for Medium Range Weather Forecasts forecasting system. *J. Geophys. Res.,* **96,** 9121–9132.

——, L. Smith, and Y. Fouquart, 1986: Pressure and temperature dependance of the absorption in longwave radiation parameterizations. *Beitr. Phys. Atmos.,* **59,** 455–469.

Neiburger, M., 1960: The relation of air mass structure to the field

of motion over the eastern North Pacific Ocean in summer. *Tellus,* **12,** 31–40.

Nicholls, S., 1984: The dynamics of stratocumulus. *Quart. J. Roy. Meteor. Soc.,* **110,** 821–845.

Paluch, I. R., and D. H. Lenschow, 1991: Stratiform cloud formation in the marine boundary layer. *J. Atmos. Sci.,* **48,** 2141–2158.

Pawlowska, H., and J.-L. Brenguier, 2000: Microphysical properties of stratocumulus clouds during ACE-2. *Tellus,* **52B,** 868–887.

——, and ——, 2003: An observational study of drizzle formation in stratocumulus clouds for general circulation model (GCM) parameterizations. *J. Geophys. Res.,* **108,** 8630, doi:10.1029/2002JD002679.

Pincus, R., and M. Baker, 1994: Effect of precipitation on the albedo susceptibility of clouds in marine boundary layers. *Nature,* **372,** 250–252.

Radke, L. F., J. A. Coakley Jr., and M. D. King, 1989: Direct and remote sensing observations of the effects of ships on clouds. *Science,* **246,** 1146–1149.

Savic-Jovcic, V., and B. Stevens, 2008: The structure and mesoscale organization of precipitating stratocumulus. *J. Atmos. Sci.,* **65,** 1587–1605.

Savijärvi, H., and P. Räisänen, 1998: Long-wave optical properties of water clouds and rain. *Tellus,* **50A,** 1–11.

Solomon, S., D. Qin, M. Manning, M. Marquis, K. Averyt, M. M. B. Tignor, H. L. Miller Jr., and Z. Chen, Eds., 2007: *Climate Change 2007: The Physical Science Basis.* Cambridge University Press, 996 pp.

Squires, P., 1958: The microstructure and colloidal stability of warm clouds. Part I: The relation between structure and stability. *Tellus,* **10,** 256–271.

——, and T. Twomey, 1961: The relation between cloud drop numbers and the spectrum of cloud nuclei. *Physics of Precipitation, Geophys. Monogr.,* Vol. 5, Amer. Geophys. Union, 211–219.

Stevens, B., 2007: On the growth of layers of nonprecipitating cumulus convection. *J. Atmos. Sci.,* **64,** 2916–2931.

——, W. C. Cotton, G. Feingold, and C.-H. Moeng, 1998: Large-eddy simulations of strongly precipitating, shallow, stratocumulus-topped boundary layers. *J. Atmos. Sci.,* **55,** 3616–3638.

——, and Coauthors, 2003: Dynamics and chemistry of marine stratocumulus—DYCOMS-II. *Bull. Amer. Meteor. Soc.,* **84,** 579–593.

Turton, J. D., and S. Nicholls, 1987: A study of the diurnal variation of stratocumulus using a multiple mixed-layer model. *Quart. J. Roy. Meteor. Soc.,* **113,** 969–1009.

Twomey, S., 1959: The nuclei of natural cloud formation. Part II: The supersaturation in natural clouds and the variation of cloud droplet concentration. *Pure Appl. Geophys.,* **43,** 243–249.

——, 1977: The influence of pollution on the shortwave albedo of clouds. *J. Atmos. Sci.,* **34,** 1149–1152.

van Zanten, M. C., and B. Stevens, 2005: Observations of the structure of heavily precipitating marine stratocumulus. *J. Atmos. Sci.,* **62,** 4327–4342.

Vetterling, W. T., S. A., Teukolsky, W. H. Press, and B. P. Flannery, 1992: *Numerical Recipes: Example Book (C).* 2nd ed. Cambridge University Press, 325 pp.

Warner, J., 1968: A reduction of rain associated with smoke from sugar-cane fires—An inadvertent weather modification. *J. App. Meteor.,* **7,** 247–251.

——, and S. Twomey, 1967: The production of cloud nuclei by cane fires and the effect on cloud droplet concentration. *J. Atmos. Sci.,* **24,** 704–706.

Warren, S., C. Hahn, J. London, R. Chervin, and R. Jenne, 1988: Global distribution of total cloud cover and cloud type amounts over the ocean. NCAR Tech. Note NCAR/TN-317+STR, 42 pp.

Wood, R., C. S. Bretherton, and D. L. Hartmann, 2002: Diurnal cycle of liquid water path over the subtropical and tropical oceans. *Geophys. Res. Lett.,* **29,** 2092, doi:10.1029/2002GL015371.